ORIGINAL PAPER

Magnetic Fe–Cr–Ni oxide alloy nano-belts prepared from the chemical decomposition of a stainless steel screw (a top-down approach): an efficient and cheap catalyst for multicomponent reactions
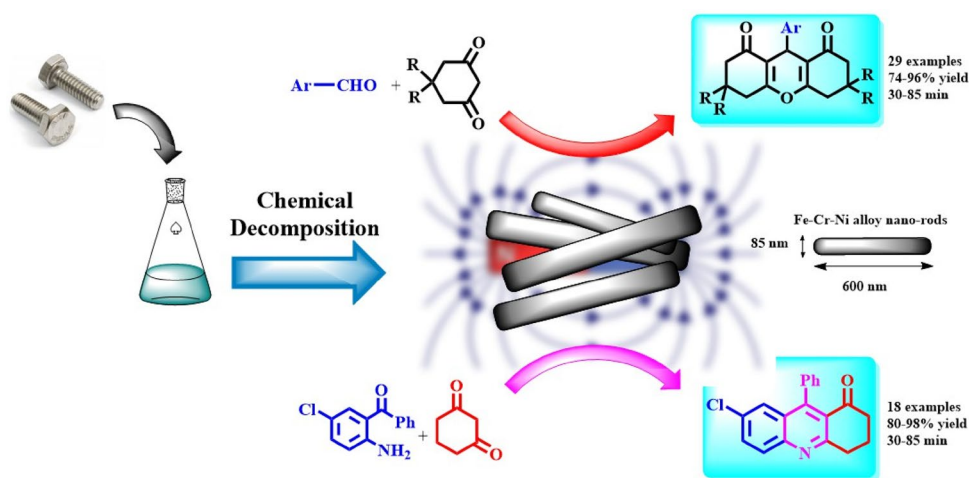
Milad Kazemnejadi[1] · Zeinab Sharafi[2] · Boshra Mahmoudi[3] · Atefeh Zeinali[1] · Mohammad Ali Nasseri[1]

Abstract

A new, cheap, and accessible method has been used for the preparation of nano-belts from the chemical decomposition (top-down approach) of a cheap stainless steel screw and found as an efficient magnetically recyclable nanocatalyst for the preparation of quinolines and 1,8-dioxo-octahydroxanthenes under mild reaction conditions. The nano-belts, Fe–Cr–Ni oxide alloy, was prepared in a two-step synthesis and characterized with various instrumental methods. Due to magnetic property of the screw (a ferritic-alloy), the resultant nano-belts is magnetic. Magnetic Fe–Cr–Ni alloy nano-belts were applied toward efficient preparation of quinolines and 1,8-dioxo-octahydroxanthenes under mild conditions. The catalyst could be readily recovered and recycled for several consecutive runs, while it suffers from a very low metal leaching and subsequently efficiency drop.

Graphic abstract

Introduction

The top-down method is one of the most applicable strategies for the preparation of nanoparticles [1], first introduced by Feynman [1, 2] as a method for making particles in nanometer dimensions. In this method, nanoparticles are produced from larger masses of materials using shaving, milling, etc.

Mechanical alloying, nanolithography, and severe plastic deformation are three main top-down approaches for the preparation of NPs [3, 4]. However, they involve harsh reaction conditions and need expensive process (instruments, solvents, time, etc.). In this study, we are going to introduce another top-down approach for the synthesis of metal alloy nanoparticles from an oxidizing mixture solution of HNO_3/DMSO/NaOCl (HDN reagent). The present method is cheap and easy handling, which produces nanoparticles in two steps. Screw was chosen as a bulk precursor for the synthesis of NPs that was subjected to these solutions, and the prepared nano-belts were used as an efficient magnetic nanocatalyst for organic reactions.

Heterocyclic compounds received considerable attention due to various biological and chemical applications [5, 6]. Quinolines and xanthenes are two main classes of heterocycle chemistry. Quinolines constitute a most applicable class of *N*-containing heterocyclic compounds that have been caught attention of researchers due to of their broad range of biological activities such as antimicrobial, anti-inflammatory, antihypertensive, anti-asthmatic, anticancer, and antimalarial [7]. Quinolines can be found in natural products (especially in alkaloids), shale oil, petroleum, wood preservation, and coal processing [8]. Various methodologies have been developed for the preparation of quinolines for sake of their inevitable applications in biological and organic synthesis such as: Combes, Pfitzinger, Conrad–Limpach, Skraup, Doebner–von Miller, and Friedländer annulation. Friedländer annulation is the most popular and straightforward approach for the preparation of quinolines that involves condensation cyclization between an active carbonyl compound containing an active α-methylene group and 2-aminoaryl ketones [9]. The reaction could be catalyzed by a variety of acid-based catalysts or transition metal-based catalytic systems that can be point to some recently: (1) microwave [10], (2) malic acid [11], (3) $[MoO_2]^{2+}$ [12], (4) $[Mn(CO)_5Br]$ [5], (5) α-Chymotrypsin [7], (6) sulfonyl imidazolium salt [13], (7) $Fe_3O_4@SiO_2@ZnCl_2$ [14], (8) benzylamine [8], (9) carbon aerogel [15], and (10) calcium silicate nanoparticles [16].

Xanthene is another important class of heterocyclic compounds that contains the pyran ring. Numerous biological activities have been known for them such as anti-bacterial, anti-inflammatory, anti-viral, photodynamic therapy, antiplasmodia, and laser technology [6, 17, 18]. Also, they played a vital role in other fields of science such as agricultural, industrial, material science, and medicinal chemistry [19, 20]. Xanthene ring can be constructed via various methods including: (1) Knoevenagel–Michael reaction of two equivalents of 1,3-cyclohexadione with aldehydes (2) cyclocondensation reaction of 2-hydroxyaromatic aldehydes and 2-tetralone [21], (3) the reaction of benzaldehyde and acetophenone [22], and (4) the condensation of β-naphthol with

alkyl or aryl aldehydes [23] in acidic conditions. Among them, multicomponent domino Knoevenagel–Michael reaction of two equivalents of 1,3-cyclohexadione with aldehydes [6] is the most current approach for the synthesis of xanthenes in the presence of various types of catalysts such as: Lewis acids [20], ZrO_2 [24], $SmCl_3$ [25], $Fe_3O_4@SiO_2$-HPW (HPW = phosphotungstic acid) [26], tetrapropylammonium bromide (TPAB) [27], silica sulfuric acid [19], sulfonated starch nanoparticles [28], ultrasound [29], $Fe_3O_4@SiO_2@GMSI$-VB1-Ni^{2+} (GMSI = (3-glycidyloxypropyl) trimethoxysilane; VB1 = covalent bonding of thiamine [17], CuS quantum dots [30], sulfated polyborate [31], nano-TiO_2 [32], $Fe_3O_4@SiO_2$–SO_3H [33], and *N*-sulfonated DABCO (DABCO = 1,4-diazabicyclo[2.2.2]octane) [34]. Very recently, Kim and co-workers reported the catalyst-free synthesis of xanthenes in a water–ethanol medium [18].

Despite considerable progress in synthesis of quinolines and 1,8-dioxo-octahydroxanthenes, they suffer from numerous drawbacks including low yields, tedious work-up, long reaction times, use of expensive and toxic reagents, and are not environmentally friendly.

Herein, in accordance with green chemistry consideration as well as economical and industrial aspects, we have reported a cheap magnetic nanocatalyst Fe–Cr–Ni oxide alloy that is prepared by the chemical decomposition of a stainless steel screw with easily accessible and high catalytic activity for the construction of quinoline as well as xanthene derivatives in water as a green solvent at room temperature.

Experimental

Materials and instrumentation

A carbon alloy of screw (ferritic stainless steel 304) with 25 mm height, 4.0 mm width, 2.223 g, was purchased from PICHSASAN ARAS IRANIAN Co., and used for the chemical decomposition and subsequently catalyst preparation. All solvents and reagents were in analytical grade and provided from Sigma and Fluka companies. Reactions progress was monitored by thin layer chromatography (TLC). FTIR spectra were recorded using a JASCO FT/IR 4600 spectrophotometer using KBr pellet. The ^1H NMR and ^{13}CNMR spectra were recorded on a Bruker AVANCE III 300 MHz spectrometer in $CDCl_3$ and DMSO-d_6 as a solvent and TMS as an internal standard. Field emission scanning electron microscopy (FE-SEM) images were obtained on a FEI NOVA NanoSEM 450. EDX spectroscopy was performed using field emission scanning electron microscope (FE-SEM, JEOL 7600F), equipped with a spectrometer of energy dispersion of X-ray from Oxford instruments. XPS studies were conducted using an XR3E2 (VG Microtech) twin anode X-ray

source with Al Kα = 1486.6 eV. Transmission electron microscopy (TEM) was performed on a Philips EM208 microscope and was operated at 100 kV. DLS analysis for the nano-belts was performed on a HORIBA-LB550 instrument. The data were analyzed by DTS applications 5.10 software. The detection angle was 90 °C for the size measurement, and the intensity average particle size of the nano-belts was measured by a nonnegative least squares analysis method [35]. TGA of the samples has been performed on a NETZSCH STA 409 PC/PG in nitrogen atmosphere with a heating rate of 10 °C/min in the temperature range of 25–1000 °C. The magnetic behavior of the samples was conducted on Lake Shore vibrating sample magnetometer (VSM) at room temperature. The surface area, pore volume, and pore diameter of the obtained NPs were determined by N_2 physisorption at − 196 °C with surface area and pore size analyzer (Micromeritics ASAP 2000 instrument) using the BET method. Metal leaching studies were performed using an inductively coupled plasma mass spectrometer (ICP-MS) Thermo Elemental VG PQ ExCell. XRF analysis was carried out by a XRF Philips PW1730 instrument. The surface area, pore volume, and pore diameter of the obtained NPs were determined by N_2 physisorption at − 196 °C with surface area and pore size analyzer (Micromeritics ASAP 2000 instrument) using the BET method.
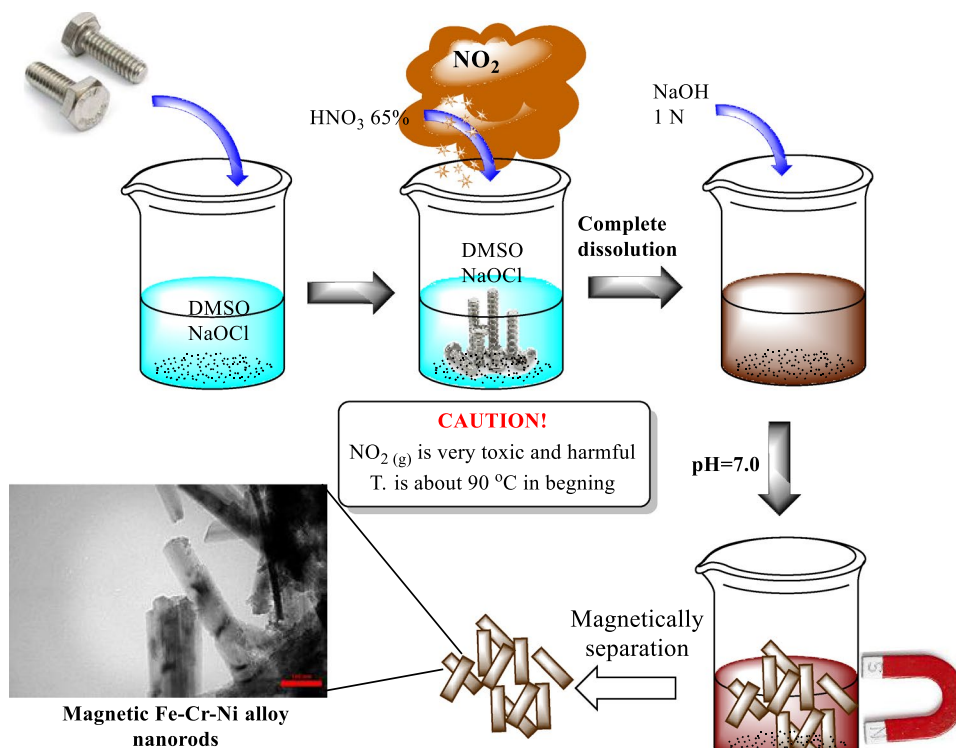
Preparation of the catalyst

In a 100 mL beaker, a ferritic stainless steel-304 with 2.223 g in weight was placed and 5 mL DMSO and 5 mL NaOCl solution were added (Fig. 1). Then, 10 mL HNO_3 65% was added to the solution. Immediately after the addition, a red color of NO_2 gas was generated and chemical decomposition/corrosion of the screw was started. The temperature remained constant at 75 °C during decomposition, so that the boiling solution was quite clear (no external heating was applied). The decomposition continued to complete dissolution of the screw, and a transparent dark brown solution was obtained (no suspensions or gels are formed). The complete dissolution takes 35 min. The resultant solution was centrifuged to eliminate any unreacted metal screw. Then, the solution was neutralized with NaOH 1 N. Upon neutralization, the dark brown sediment was obtained. The precipitate was washed several times with deionized water (2×20 mL) and EtOH (2×20 mL), dried into oven (60 °C), and isolated as a stable powder at room temperature in air atmosphere. An experimental view for the preparation of the catalyst is shown in Fig. 1.

Typical procedure for preparation of 1,8-dioxo-octahydroxanthenes

To a 25 mL round bottom flask, benzaldehyde (1.0 mmol) and dimedone (2.2 mmol) were added to 2 mL of water.

Fig. 1 An experimental schematic for the preparation of the magnetic Fe–Cr–Ni alloy nanoparticles

Magnetic Fe-Cr-Ni alloy nanorods

The catalyst (5 mg) was added to the mixture, and the resulting mixture was stirred for the appropriate time at room temperature. The reaction progress was monitored by TLC. Upon reaction completion, 5 mL ethanol was added to the mixture and the catalyst was separated by an external magnetic field. Then, the product was extracted with EtOAc (3×7 mL). The organic phases were combined, and the solvent was removed under reduced pressure. The crude product was recrystallized from EtOH to afford the pure xanthene product.

Typical procedure for preparation of quinolines

In a typical procedure, to a 25 mL round bottom flask, 2-aminobenzophenone (1.0 mmol) and dimedone (1.2 mmol) were added to 3 mL of water. The catalyst (5 mg) was added to the mixture, and the resulting mixture was stirred at room temperature for an appropriate time. The reaction progress was monitored by TLC. Upon the reaction completion, 5 mL of ethanol was added to the mixture and the catalyst was separated by an external magnetic field. Then, the product was extracted with EtOAc (7 mL × 3). The organic phases were combined, and the solvent was removed under reduced pressure. The crude product was recrystallized with EtOH to afford the pure quinoline product.

Results and discussion

Catalyst characterization

The prepared nano-belts were characterized by various spectroscopic methods. FTIR spectrum represents a series of peaks at 444–681 cm^{-1} that could be assigned to Fe–O, Cr–O or Ni–O stretching vibrations [36, 37]. This is completely in agreement with magnetic behavior of the NPs. A peak at 1624 cm^{-1} demonstrates the vibration of water trapped in nano-belts (Fig. 2a).

The nanoparticles represent a superparamagnetic behavior with saturation magnetization of 65 emu g^{-1} (Fig. 2b). This behavior could be attributed directly to the Fe$_3$O$_4$ phases in the nano-belts in accordance with the FTIR spectrum. The NPs represent an excellent thermal stability, which there is not found any noticeable weight loss until 1000 °C. This behavior exhibited that the NPs are completely inorganic in nature and there are not any decomposable organic compounds in the NPs. A small weight loss of ~2% at temperature below 200 °C is related to desorption of water that is trapped in the network of NPs (Fig. 2c).

From XRD pattern of nano-belts, various phases including Fe$_3$O$_4$, CrO$_2$, and NiO could be seen. The peaks appeared at $2\theta = 29.7°$, 36.6°, 43.3°, 53.5°, and 62.9°
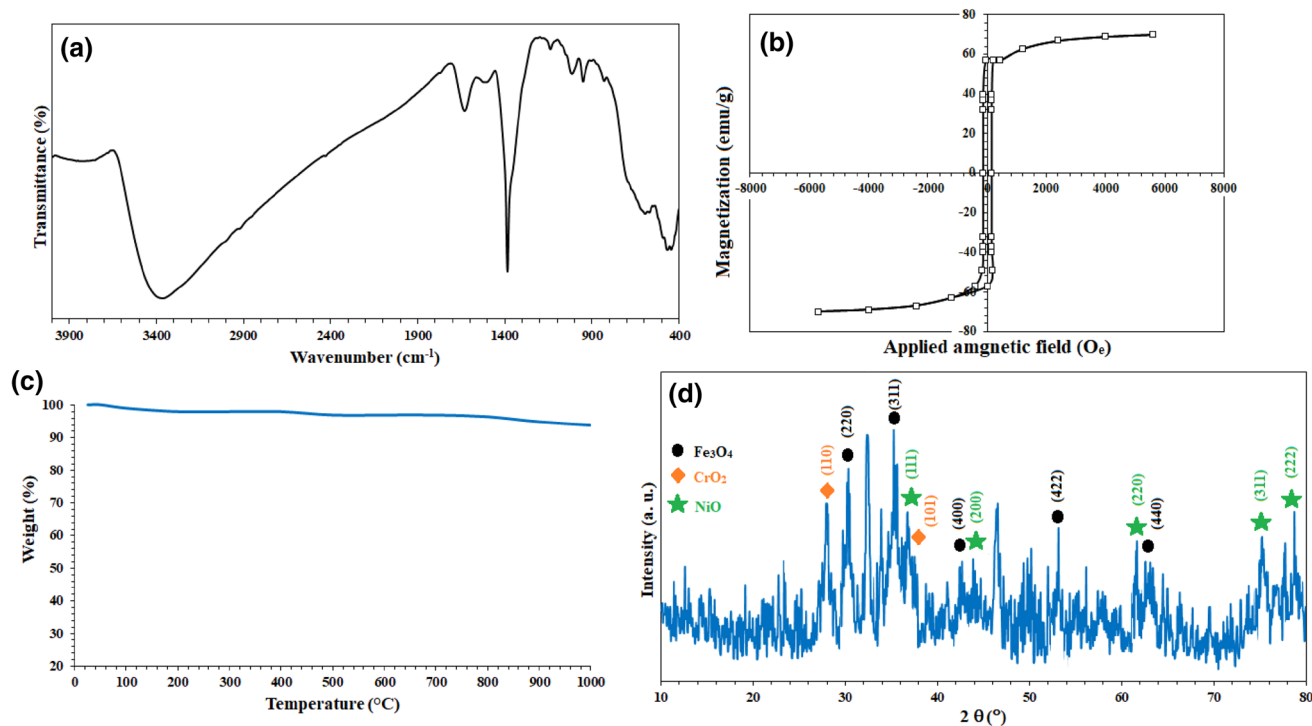

Fig. 2 FTIR spectrum (**a**), **b** VSM curve, **c** TGA curve, and **d** XRD spectrum of the Fe–Cr–Ni oxide alloy nanoparticles

correspond to the (220), (311), (400), (422), (440) planes that are related to the inverse spinel crystal structure of Fe_3O_4 (Fig. 2d, black circles) [38]. The characteristic diffraction peaks at $2\theta = 37.3°$, $43.5°$, $62.5°$, $75.6°$, and $78.4°$ could be marked, respectively, by their indices to the (111), (200), (220), (311), and (222) planes, demonstrating NiO structure [39]. Moreover, two peaks at $2\theta = 27.6°$ and $36.8°$ could be assigned to CrO_2 crystal structure and correspond to (110) and (101) planes, respectively [40].

Morphology and shape of the NPs were identified from SEM and TEM images. As shown in Fig. 3, the nanoparticles are belt-like in shape with a homogenous morphology. The nano-belts have an average size of 85 nm.

The EDX analysis demonstrated the presence of C, O, Fe, Cr, Ni, Si, and Mn elements in the nano-belts in agreement with a ferritic stainless steel 304 chemical composition (Fig. 4a). Also, the major components were Fe, O, Cr, and Ni with 37.58, 44.33, 12.87, and 3.60 wt%, respectively (Fig. 4a-inset table). The presence of the elements was also confirmed by XPS analysis of the nano-belts completely in agreement with the EDX analysis. The corresponding bonding energies are assigned in Fig. 4b. The result from XRF analysis did not show any other heavy metals that were

detected by XPS and EDX analyses (Fig. 4c). Although the determination of particles size distribution of nano-belts is challenging due to non-spherical shape, but Liu et al. [35] introduced an efficient reliable method for this measurement, where the particles size distribution of the nano-belts was measured using a fixed angle DLS. The results were in agreement with those from TEM, and the nano-belts have a mean size of 85 nm with a sharp-narrow peak (Fig. 4d). As shown in Fig. 4d, a nearly symmetrical size distribution was obtained for the nano-belts. The specific surface area and porosity of the nano-belts were studied by N_2 adsorption–desorption isotherm analysis. Based on the BET isotherm, specific surface area and pore volume of the nano-belts were obtained 186 m^2/g and 1.619 cm^3/g, respectively (Table 1).

$2p$ High-resolution XPS analysis was performed to investigate the detailed elemental information and the oxidation state of Fe–Cr–Ni oxide alloy. Figure 5a-d shows the binding energies related to Cr$2p$, Mn$2p$, Fe$2p$, and Ni$2p$. Cr $2p$ XPS spectrum of the alloy and clearly proved the presence of CrO_2 phases with their corresponding binding energies at 576.4 eV (Cr $2p_{3/2}$) and 586.4 eV (Cr $2p_{1/2}$) in agreement with the literature (Fig. 5a) [41, 42]. High-resolution XPS
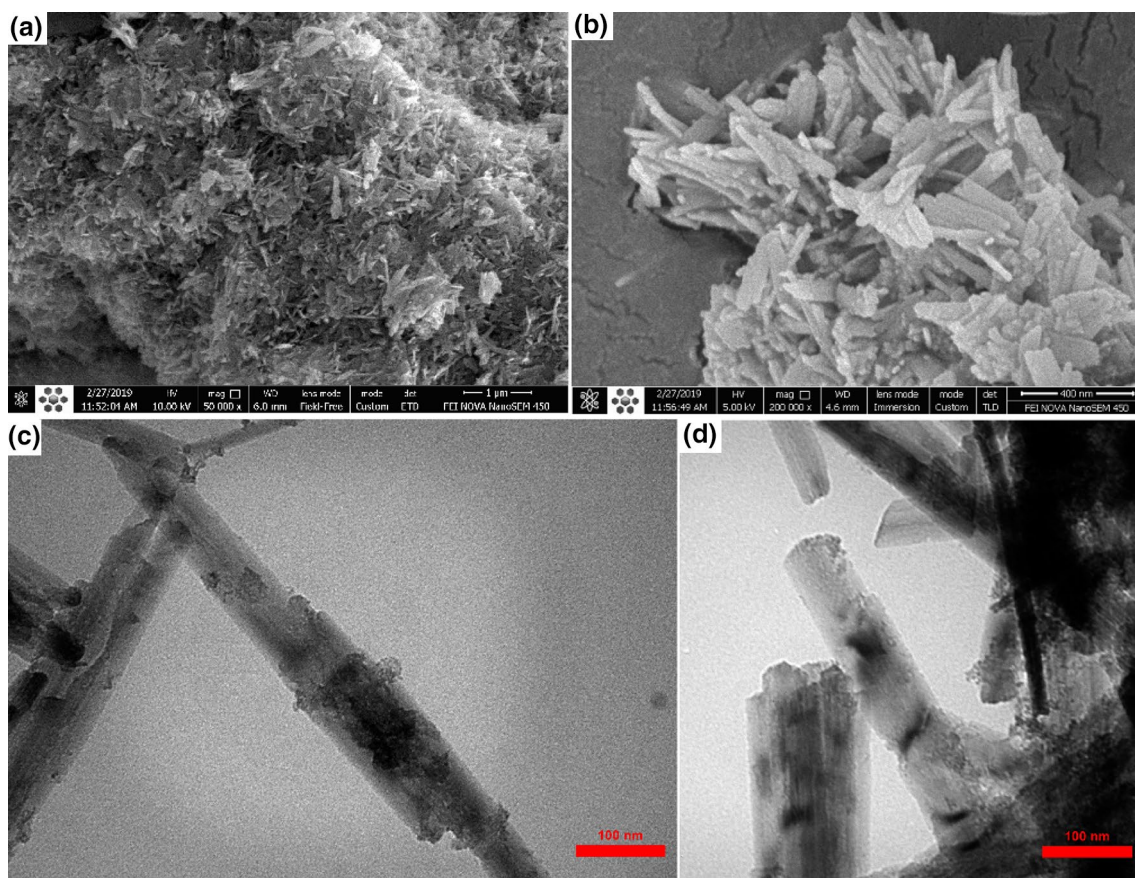

Fig. 3 SEM (**a**, **b**), and TEM (**c**, **d**) images of Fe–Cr–Ni oxide alloy nanoparticles
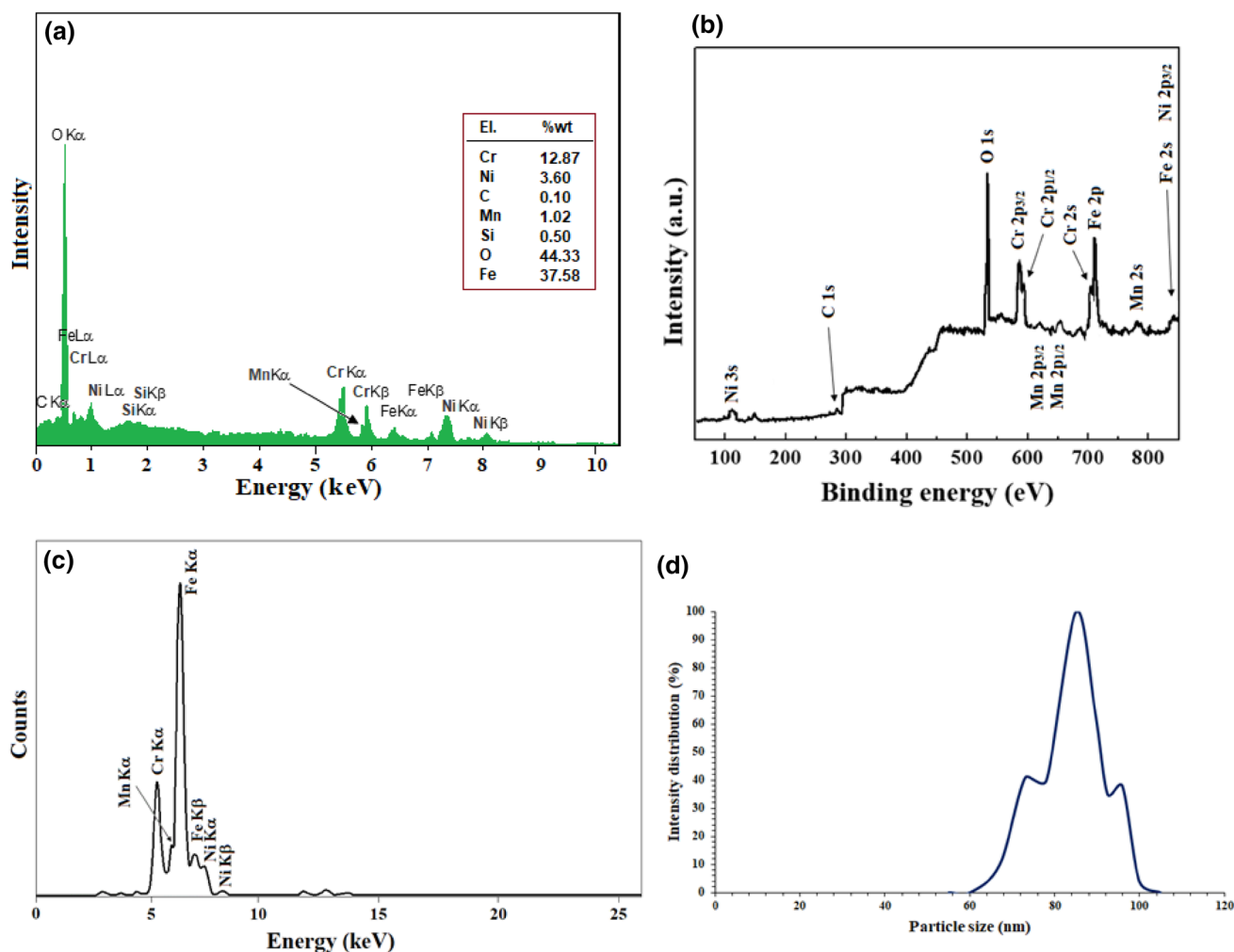
Fig. 4 EDX (**a**), XPS (**b**), XRF (**c**), and DLS (**d**) spectra of the Fe–Cr–Ni alloy nanoparticles

Table 1 Surface characteristics of Fe–Cr–Ni oxide alloy

XRD crystalline size (mn)	TEM particle size (nm)	Specific surface area (m²/g)	Pore volume (cm³/g)	Average pore radius (nm)
69	85	186	1.619	2.577

spectrum of Mn 2p showed two couples characteristic peaks at (640.5, 652.0 eV) and (642.0, 653.0) related to (Mn 2$p_{3/2}$, Mn 2$p_{1/2}$) for Mn^{3+} and Mn^{4+}, respectively (Fig. 5b) [43]. Although the Mn content in the alloy is very low (1.02 wt% based on EDX analysis), the presence of Mn oxides, Mn_2O_3, and MnO_2 is likely due to the presence of +3 and +4 nuclei in the alloy (Fig. 5b). For the Fe 2p XPS spectrum, two spin–orbit splitted represent the existence of both Fe^{2+} and Fe^{3+} in Fe_3O_4 phases (Fig. 5c) [44]. The peaks at 710.0 (2$p_{3/2}$) and 723.4 (2$p_{1/2}$) eV correspond to Fe^{2+}, and 711.8 (2$p_{3/2}$) and 725.5 (2$p_{1/2}$) eV are related to Fe^{3+} [45]. The

Ni 2p spectrum represents two edge splits by spin orbital coupling including 2$p_{3/2}$ and 2$p_{1/2}$ at ~854 and ~872 eV, respectively (Fig. 5d). Also, their corresponding satellites were appeared at 862.1 and 879.0 eV, respectively, which confirmed the existence of NiO phases in Fe–Cr–Ni oxide alloy [46, 47].

Catalytic activity

In order to investigate the parameters involved in the reaction, the reaction of benzaldehyde with dimedone was chosen as a model reaction for the preparation of 9-phenyl-3,4,5,6,7,9-hexahydro-1*H*-xanthene-1,8(2H)-dione. First of all, the reaction was conducted in various types of solvents (Table 2). The best choice was water as a green solvent with 90% conversion at room temperature; although some other solvents such as EtOH, PEG-200, glycerol, and DMSO afforded same and/or slightly higher conversion, since environmental and industrial aspects, water was selected
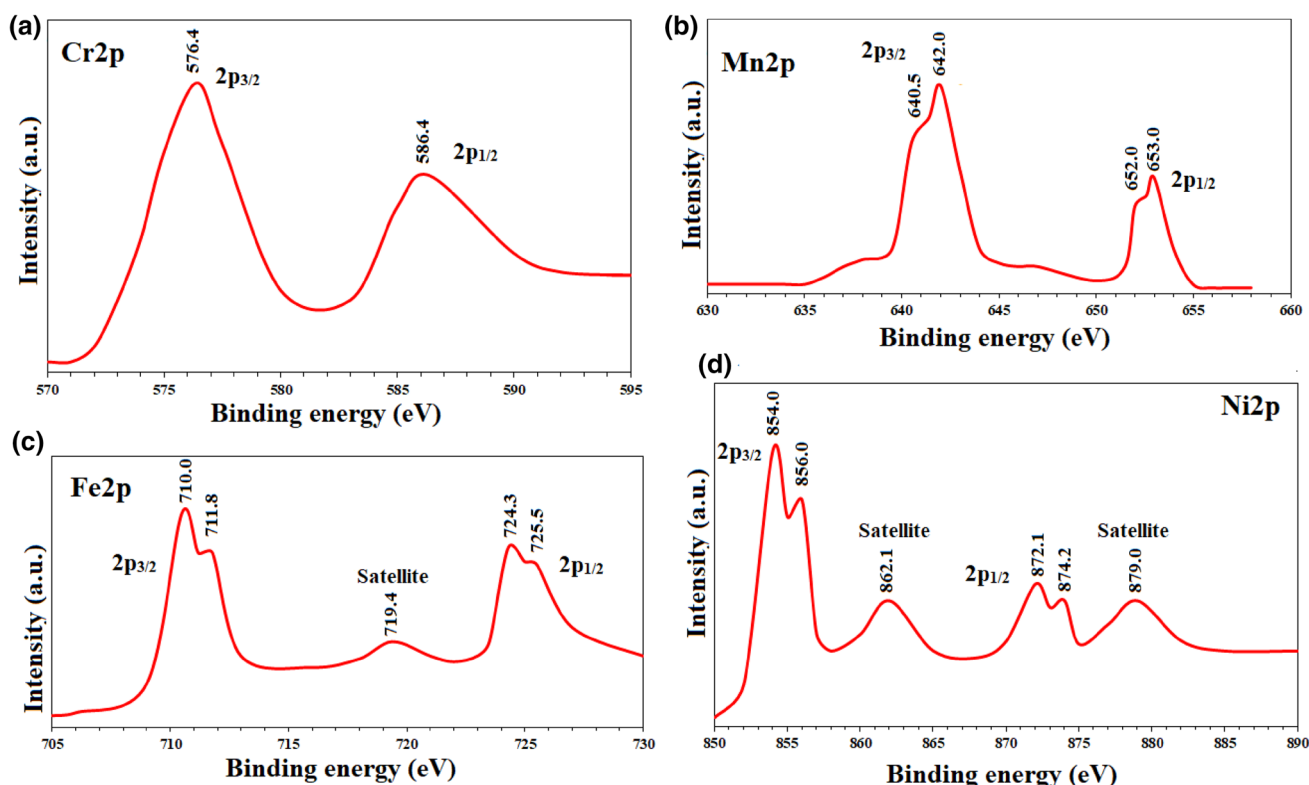
Fig. 5 High-resolution XPS (energy-corrected) analysis of Fe–Cr–Ni oxide alloy: **a** Cr 2*p*, **b** Mn 2*p*, **c** Fe 2*p*, and **d** Ni 2*p*

Table 2 Optimization experiments for the reaction of benzaldehyde, dimedone catalyzed by Fe–Cr–Ni alloy

Entry	Solvent	Cat. amount (mg)	Time (min)	Yield (%)
1	H$_2$O	5.0	65	90
2	EtOH	5.0	65	90
3	DMSO	5.0	65	92
4	Glycerol	5.0	80	90
5	PEG-200	5.0	80	88
6	CH$_3$CN	5.0	120	75
7	DEE	5.0	120	45
8	H$_2$O	3.0	80	65
9	H$_2$O	4.0	80	85
10	H$_2$O	6.0	80	90
11	H$_2$O	8.0	80	91
12	H$_2$O	–	180	Trace

Reaction conditions: dimedone (2.2 mmol), benzaldehyde (1.0 mmol), catalyst, solvent (3.0 mL), room temperature
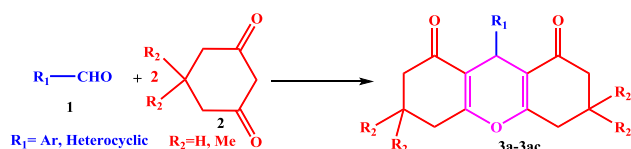
as the premium solvent in our study. The highest possible efficiency was obtained in the presence of only 5.0 mg of catalyst in water, which give 90% conversion for 65 min (Table 2).

All experiments were performed at room temperature; it should be noted that the increase in temperature did not cause a noticeable change in efficiency. The vital role of the catalyst was elucidated when the reaction was carried out in the absence of the catalyst, and a trace amount was obtained (Table 2).

After finding the optimum conditions for the preparation of xanthene compounds, various derivatives of aldehyde were condensed with dimedone or 1,3-cyclohexadione in the presence of 5.0 mg of catalyst in water at room temperature. The results are tabulated in Table 3. As shown in Table 3, a wide scope of aldehyde-bearing electron-donating group (**3b**, **3c**, **3g**, **3h**, **3u**, **3v**, …) or electron-withdrawing group (**3d**, **3e**, **3i**, **3j**, **3o**, **3p**, …) could be transferred to xanthenes with high efficiency (74–96%, 30–85 min). This diversity reflects the compatibility of the catalyst toward a variety of functional groups, which acid sensitive aldehydes such as thiophene-2-carbaldehyde (Table 3, entry 12) and furfural (Table 3, entry 13) could be efficiently transformed to the corresponding xanthenes.

Encouraged by the obtained results from the preparation of xanthenes, we then examined the versatility and generality of this method toward the preparation of quinolines. As shown in Table 4, again, a wide variety of carbonyl compounds whether aliphatic or aromatic (**5**) were condensed with 2-aminobenzophenone and/or 2-amino-5-chlorbenzophenone (**4b**), and high to excellent yields were achieved for all of entries.
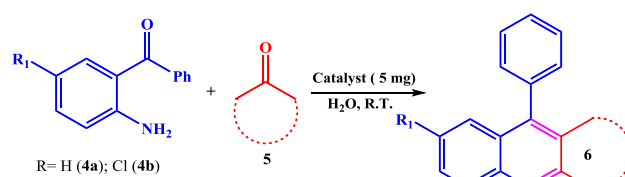
Table 3 Preparation of 1,8-dioxo-octahydroxanthenes (**3a–3ac**) catalyzed by Fe–Cr–Ni nano-belts in water at room temperature

Entry	R_1	R_2	Product	Time (min)	Yield (%)
1	Phenyl	H	**3a**	65	90
2	4-Me-phenyl	H	**3b**	50	88
3	4-OMe-phenyl	H	**3c**	55	86
4	4-Cl-phenyl	H	**3d**	70	82
5	3-Cl-phenyl	H	**3e**	50	92
6	3-Me-phenyl	H	**3f**	45	90
7	2-OH-phenyl	H	**3g**	50	86
8	4-OH-phenyl	H	**3h**	45	89
9	4-NO$_2$-phenyl	H	**3i**	35	97
10	3-NO$_2$-phenyl	H	**3j**	30	97
11	Phenyl	Me	**3k**	60	96
12	2-Thiophene	Me	**3l**	70	98
13	2-Furyl	Me	**3m**	60	98
14	2,5-diMeO-phenyl	Me	**3n**	60	80
15	2-Pyridil	Me	**3o**	60	96
16	3-Pyridil	Me	**3p**	60	98
17	2-Naphthyl	Me	**3q**	80	76
18	4-Me-phenyl	Me	**3r**	45	79
19	2-NO$_2$-phenyl	Me	**3s**	85	89
20	3-Me-phenyl	Me	**3t**	60	73
21	2-OH-phenyl	Me	**3u**	80	76
22	4-OH-phenyl	Me	**3v**	40	82
23	4-Br-phenyl	Me	**3w**	55	83
24	4-Cl-phenyl	Me	**3x**	80	74
25	4-I-phenyl	Me	**3y**	45	94
26	2-MeO-phenyl	Me	**3z**	80	78
27	4-NO$_2$-phenyl	Me	**3aa**	75	90
28	3-NO$_2$-phenyl	Me	**3ab**	40	96
29	4-MeO-phenyl	Me	**3ac**	85	85

Reaction conditions: 1,3-dione (2.2 mmol), aldehyde (1.0 mmol), catalyst (5.0 mg), water (3.0 mL), room temperature

Recyclability studies

The main advantage of a heterogeneous catalyst is its ability to recover from the reaction medium and use it repeatedly without compromising efficiency [36, 37, 48]. This property is very important in terms of economic, industrial objectives, and environmental sustainability. In this way, both reactions of (1) dimedone with benzaldehyde (preparation of **3a**), and (2) 2-aminobenzophenone with 1,3-cyclohexadione (preparation **6a**) were performed several consecutive times under

Table 4 Preparation of quinoline derivatives (**6a–6r**) catalyzed by Fe–Cr–Ni nano-belts in water at room temperature

Entry	**4**	**5**	Product	Time (min)	Yield (%)
1	**4a**	1,3-Cyclohexanone	**6a**	50	90
2	**4a**	Methyl acetoacetate	**6b**	35	98
3	**4a**	Cycloheptanone	**6c**	38	98
4	**4a**	Acetophenone	**6d**	35	95
5	**4b**	Ethyl acetoacetate	**6e**	60	85
6	**4b**	1,3-cyclohexanone	**6f**	40	88
7	**4a**	4′-MeO-acetophenone	**6g**	32	98
8	**4a**	4′-OH-acetophenone	**6h**	35	92
9	**4b**	4′-Cl-acetophenone	**6i**	50	88
10	**4a**	4′-NO$_2$-acetophenone	**6j**	50	86
11	**4a**	Cyclohexanone	**6k**	60	95
12	**4b**	4′-Cl-acetophenone	**6l**	40	98
13	**4a**	Cyclopentanone	**6m**	45	93
14	**4b**	Acetophenone	**6n**	66	86
15	**4b**	Acetylacetone	**6o**	85	82
16	**4b**	Dimedone	**6p**	30	97
17	**4a**	Acetylacetone	**6q**	40	80
18	**4a**	4′-Cl-acetophenone	**6r**	30	80

Reaction conditions: 2-aminobenzophenone (1.0 mmol), carbonyl compound (1.2 mmol), catalyst (5.0 mg), water (3.0 mL), room temperature
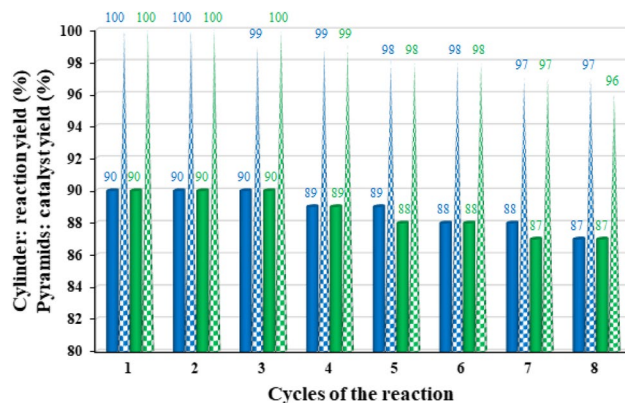

Fig. 6 Studies of recycling of the catalyst during the successive reaction cycles for the preparation of **3a** and **6a**

Table 5 Measurement of leaching amount in each reaction cycle for the reaction of benzaldehyde and dimedone for the preparation of **3a**

Element	Leaching amount in each run ($\mu g\ L^{-1}$)							
	Run 1	Run 2	Run 3	Run 4	Run 5	Run 6	Run 7	Run 8
Cr	0.000	0.000	0.000	0.000	0.000	0.000	0.000	0.006
Ni	0.000	0.000	0.000	0.000	0.000	0.000	0.000	0.005
Fe	0.000	0.000	0.000	0.000	0.000	0.000	0.000	0.000
Mn	0.000	0.000	0.000	0.000	0.000	0.000	0.000	0.008

Reaction conditions: 1,3-dione (2.2 mmol), aldehyde (1.0 mmol), catalyst (5.0 mg), water (3.0 mL), room temperature

The analyses for Cr, Ni, Fe, and Mn were taken at 205.552 nm, 231.604 nm, 259.940 nm, and 257.610 nm, respectively

optimized conditions. Figure 6 shows the corresponding results that insignificant loss in efficiency was observed at the eighth run. There is only a 3% loss in product yield was achieved for both reactions (Fig. 6). In addition, metal leaching in the catalyst was studied for the reaction of dimedone with benzaldehyde (preparation of **3a**). Due to the presence of various transition metals in the catalyst, the leaching was determined for each of them in every cycle. Table 5 shows these amount for Cr, Ni, Mn, and Fe, which there are not significant. However, an ignorable amount was detected for the elements after the eight run except Fe (Table 5). To support these results, the hot filtration test was applied for this reaction. The catalyst was magnetically filtered from the reaction mixture of benzaldehyde and dimedone after 30 min at room temperature. The efficiency was 49% (GC) in this time. The reaction was allowed to proceed for another 1 h, where the
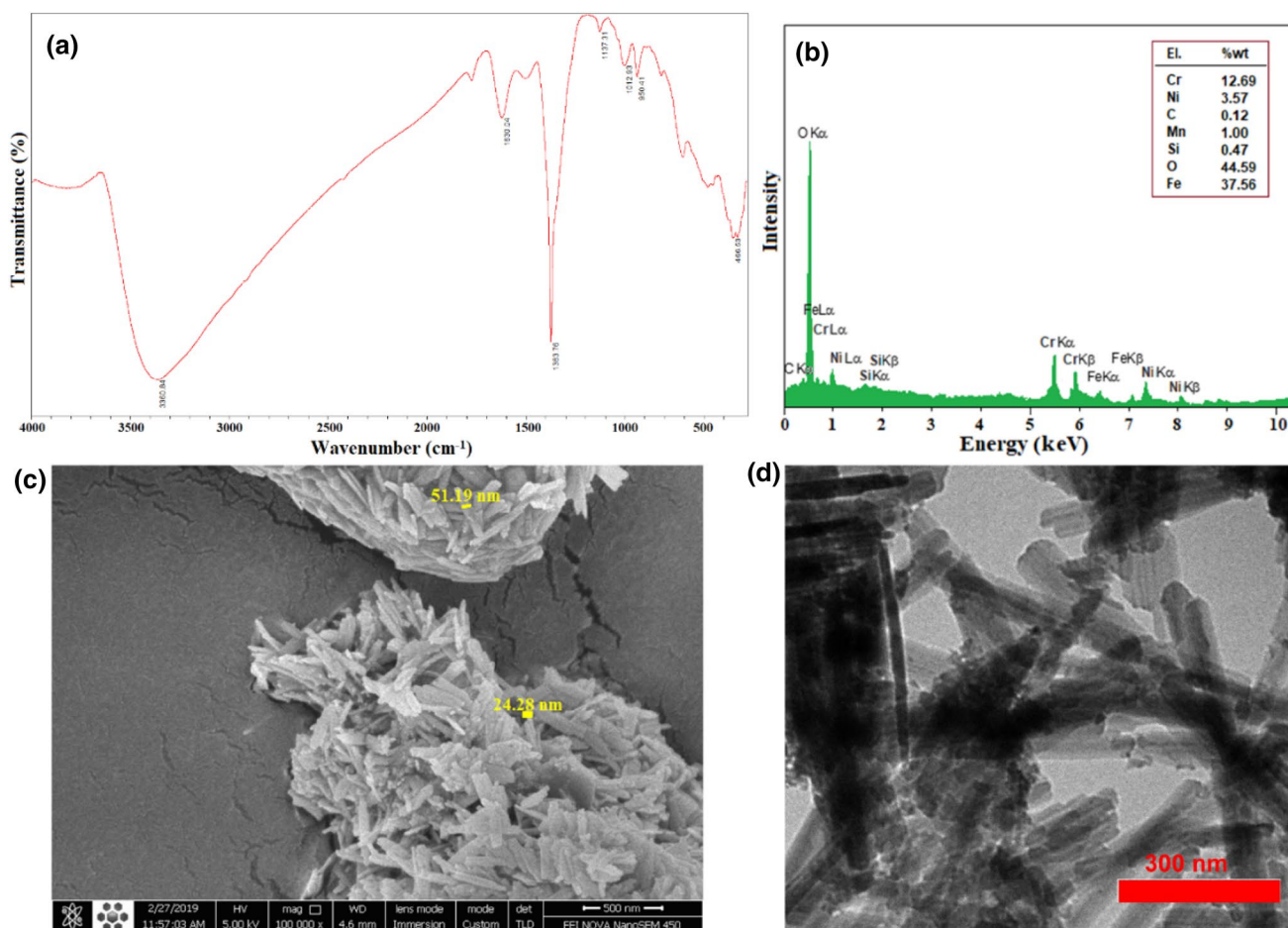

Fig. 7 FTIR (**a**) and EDX (**b**) spectra, SEM (**c**) and TEM (**d**) images of the Fe–Cr–Ni oxide alloy nanoparticles

yield reached to 50%. This indicates that the catalyst acts heterogeneously and it does not suffer any metal leaching during the reaction. These results reflect the heterogeneous nature of the catalyst which maintains its catalytic activity during recycling.

To show the stability and durability of the catalyst, it was characterized after the eight recycling test (Figs. 6 and 7). As shown in Fig. 7 and with the comparison with the fresh ones, the FTIR and EDX spectra as well as SEM and TEM images confirmed that the structure of the catalyst is as same as the fresh one and there is not any change in its structure during several recycles. FTIR and EDX spectra strongly confirmed the structure and morphology of the catalyst. Also, from the recovered SEM and TEM spectra, it could be concluded that the structure and morphology of the catalyst remain intact during the recycles (Fig. 7a–d).

Conclusion

A new approach for the top-down preparation of nanoparticles has been developed via the chemical decomposition of bulk metal alloys using the $NaOCl/HNO_3/DMSO$ reagent as an extraordinary oxidizing/corrosion mixture. In this study, magnetic Fe–Cr–Ni oxide nano-belts were prepared by chemical decomposition of a ferritic stainless steel-304 in two steps. The nano-belts demonstrated an excellent catalytic activity toward the preparation of quinolines and 1,8-dioxo-octahydroxanthenes in water at room temperature, which high to excellent yields were obtained for all compounds. The nano-belts have a diameter of about 80 nm and have sufficient magnetization of 65 emu g^{-1}, and also high thermal and mechanical resistance. The catalyst could be recycled for at least eight consecutive runs without any significant loss in its activity.

Compliance with ethical standards

Conflict of interest There are no conflict to declare.

References

1. D.G. Shchukin, G.B. Sukhorukov, Adv. Mater. **16**(8), 671–682 (2004)
2. R.P. Feynman, Eng. Sci. **23**(8), 22–36 (1960)
3. F.E. Kruis, H. Fissan, A. Peled, J. Aerosol Sci. **29**(5–6), 511–535 (1998)
4. J. Jeevanandam, A. Barhoum, Y.S. Chan, A. Dufresne, M.K. Danquah, Beilstein J. Nanotechnol. **9**(1), 1050–1074 (2018)
5. M.K. Barman, A. Jana, B. Maji, Adv. Synth. Catal. **360**(17), 3233–3238 (2018)
6. A.H. Suja, S. Sugunan, Bull. Catal. Soc. India **2**, 194–203 (2003)
7. Z.G. Le, M. Liang, Z.S. Chen, S.H. Zhang, Z.B. Xie, Molecules **22**, 762–770 (2017)
8. S.Y. Lee, C.H. Cheon, J. Org. Chem. **83**(21), 13036–13044 (2018)
9. R. Sharma, P. Kour, A. Kumar, J. Chem. Sci. **130**(6), 73–98 (2018)
10. A.T. Garrison, Y. Abouelhassan, H. Yang, H.H. Yousaf, T.J. Nguyen, R.W. Huigens, MedChemComm **8**(4), 720–724 (2017)
11. F. Tufail, M. Saquib, S. Singh, J. Tiwari, M. Singh, J. Singh, J. Singh, New J. Chem. **41**(4), 1618–1624 (2017)
12. R. Rubio-Presa, S. Suárez-Pantiga, M.R. Pedrosa, R. Sanz, Adv. Synth. Catal. **360**(11), 2216–2220 (2018)
13. A. Singhal, P. Kumari, S.M.S. Chauhan, Curr. Organocatal. **4**(3), 182–188 (2017)
14. E. Soleimani, M. Naderi Namivandi, H. Sepahvand, Appl. Organomet. Chem. **31**(2), e3566–e3574 (2017)
15. M. Godino-Ojer, E. Soriano, V. Calvino-Casilda, F.J. Maldonado-Hódar, E. Pérez-Mayoral, Chem. Eng. J. **314**, 488–497 (2017)
16. J. Palaniraja, P. Arunachalam, U. Vijayalakshmi, M.A. Ghanem, S. Mohana Roopan, Inorg. Nano-Met. Chem. **47**(6), 946–949 (2017)
17. N. Azizi, F. Abbasi, M. Abdoli-Senejani, ChemistrySelect **3**(13), 3797–3802 (2018)
18. R.M. Naidu Kalla, R.S. Karunakaran, M. Balaji, I. Kim, ChemistrySelect **4**(2), 644–649 (2019)
19. M. Seyyedhamzeh, P. Mirzaei, A. Bazgir, Dyes Pigments **76**(3), 836–839 (2008)
20. E. Böβ, T. Hillringhaus, J. Nitsch, M. Klussmann, Org. Biomol. Chem. **9**(6), 1744–1748 (2011)
21. A. Jha, J. Beal, Tetrahedron Lett. **45**(49), 8999–9001 (2004)
22. C.W. Kuo, J.M. Fang, Synth. Commun. **31**(6), 877–892 (2001)
23. R.J. Sarma, J.B. Baruah, Dyes Pigments **64**(1), 91–92 (2005)
24. P. Bansal, N. Kaur, C. Prakash, G.R. Chaudhary, Vacuum **157**, 9–16 (2018)
25. A. Ilangovan, S. Malayappasamy, S. Muralidharan, S. Maruthamuthu, Chem. Cent. J. **5**(1), 81–87 (2011)
26. T. Ikeno, T. Nagano, K. Hanaoka, Chem. Asian J. **12**(13), 1435–1446 (2017)
27. M.A. Poursattar, S. Abdollahi, M. Ezzati, E. Nemati-Kande, J. Heterocycl. Chem. **55**(6), 1324–1330 (2018)
28. J. Safari, P. Aftabi, M. Ahmadzadeh, M. Sadeghi, Z. Zarnegar, J. Mol. Struct. **1142**, 33–39 (2017)
29. N. Mulakayala, G.P. Kumar, D. Rambabu, M. Aeluri, M.B. Rao, M. Pal, Tetrahedron Lett. **53**(51), 6923–6926 (2012)
30. P. Bansal, G.R. Chaudhary, N. Kaur, S.K. Mehta, RSC Adv. **5**(11), 8205–8209 (2015)
31. M.S. Patil, A.V. Palav, C.K. Khatri, G.U. Chaturbhuj, Tetrahedron Lett. **58**(29), 2859–2864 (2017)
32. A. Khazaei, A.R. Moosavi-Zare, Z. Mohammadi, A. Zare, V. Khakyzadeh, G. Darvishi, RSC Adv. **3**(5), 1323–1326 (2013)
33. H. Naeimi, Z.S. Nazifi, J. Nanopart. Res. **15**(11), 2026 (2013)
34. F. Shirini, M.S.N. Langarudi, M. Seddighi, O.G. Jolodar, Res. Chem. Intermed. **41**(11), 8483–8497 (2015)
35. C. Dhand, N. Dwivedi, X.J. Loh, A.N.J. Ying, N.K. Verma, R.W. Beuerman, R. Lakshminarayanan, S. Ramakrishna, RSC Adv. **5**(127), 105003–105037 (2015)
36. S. Ghiami, M.A. Nasseri, A. Allahresani, M. Kazemnejadi, React. Kinet. Mech. Catal. **126**(1), 383–398 (2019)
37. M. Kazemnejadi, Z. Rezazadeh, M.A. Nasseri, A. Allahresani, M. Esmaeilpour, Green Chem. **21**(7), 1718–1734 (2019)
38. A.R. Sardarian, M. Kazemnejadi, M. Esmaeilpour, Dalton Trans. **48**(9), 3132–3145 (2019)
39. M. Ghosh, K. Biswas, A. Sundaresan, C.N.R. Rao, J. Mater. Chem. **16**(1), 106–111 (2006)

40. J. Dai, J. Tang, H. Xu, L. Spinu, W. Wang, K. Wang, A. Kumbhar, M. Li, U. Diebold, Appl. Phys. Lett. **77**(18), 2840–2842 (2000)

41. R. Cheng, B. Xu, C.N. Borca, A. Sokolov, C.S. Yang, L. Yuan, S.H. Liou, B. Doudin, P.A. Dowben, Appl. Phys. Lett. **79**(19), 3122–3124 (2001)

42. N.F. Heinig, H. Jalili, K.T. Leung, Appl. Phys. Lett. **91**(25), 253102–253104 (2007)

43. M. Kazemnejadi, S.A. Alavi, Z. Rezazadeh, M.A. Nasseri, A. Allahresani, M. Esmaeilpour, J. Mol. Struct. **1186**, 230–249 (2019)

44. F. Han, L. Ma, Q. Sun, C. Lei, A. Lu, Nano Res. **7**(11), 1706–1717 (2014)

45. R. Madhuvilakku, S. Alagar, R. Mariappan, S. Piraman, Sens. Actuators B **253**, 879–892 (2017)

46. W. Huang, S. Ding, Y. Chen, W. Hao, X. Lai, J. Peng, J. Tu, Y. Cao, X. Li, Sci. Rep. **7**(1), 5220–5231 (2017)

47. P.T. Babar, A.C. Lokhande, M.G. Gang, B.S. Pawar, S.M. Pawar, J.H. Kim, J. Ind. Eng. Chem. **60**, 493–497 (2018)

48. M. Kazemnejadi, A.R. Sardarian, RSC Adv. **6**(94), 91999–92006 (2016)

Affiliations

Milad Kazemnejadi[1] · Zeinab Sharafi[2] · Boshra Mahmoudi[3] · Atefeh Zeinali[1] · Mohammad Ali Nasseri[1]

[1] Department of Chemistry, Faculty of Sciences, University of Birjand, Birjand 97175-615, Iran

[2] Razi Herbal Medicines Research Center, Lorestan University of Medical Sciences, Khorramabad, Iran

[3] Research Center, Sulaimani Polytechnic University, Sulaimani 46001, Kurdistan Region, Iraq